Heliyon 10 (2024) e31789

Contents lists available at ScienceDirect

Heliyon

journal homepage: www.cell.com/heliyon

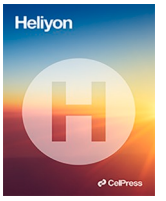

Research article

Antimicrobial poly (1,4-butylene carbonate): Preparation, characterization, and potential applications as a material for tympanic membrane repair

Yuan Lv [a], Linrong Wu [a], Jiangyu Yan [a], Zhisen Shen [a], Junjun Zhang [b,*], Xiaoqin Zhang [c,**], Tian Li [d]

[a] The Department of Otolaryngology, Head and Neck Surgery, Ningbo Medical Center Lihuili Hospital, Ningbo, Zhejiang, China
[b] Department of Trauma Surgery, Yinzhou No.2 Hospital, Ningbo, Zhejiang, China
[c] Ningbo Institute of Materials Technology and Engineering, Chinese Academy of Sciences, Ningbo, Zhejiang, China
[d] Fourth Military Medical University School of Basic Medicine, Xi'an, China

ARTICLE INFO

Keywords:
poly (1,4-butylene carbonate)
Levofloxacin
Scaffold
Tympanic membrane

ABSTRACT

Perforation of the tympanic membrane (TM) is a common condition that often requires a scaffold as a support for surgery. However, because of the external environment of the auditory canal, the scaffold could become bacterially infected and prevent the TM from healing. As a result, the perfect scaffold should have both antibacterial and biomimetic qualities. In this study, the biodegradable biomaterial poly(1,4-butylene carbonate) (PBC) films containing levofloxacin (LEV) was successfully prepared for the first time. The results showed that the hydrophilicity of the LEV/PBC film was improved after the addition of LEV, and the tensile strength was also complied with the requirements of the standard. The created antibacterial film demonstrated excellent antibacterial properties. In vitro hemolysis experiments revealed no risk of hemolysis for the new material, and the cytotoxicity study further confirmed its non-cytotoxic nature. Overall, LEV was a good component of PBC/LEV film, which is expected to be used for TM repair in the future.

1. Introduction

The tympanic membrane (TM) is a crucial structure located between the outer ear and middle ear in the human auditory system. It is a thin membrane, typically circular or oval in shape, composed of fibrous tissue and elastic fibers. The TM is positioned at the end of the ear canal, separating the outer ear from the middle ear, and it is a protective barrier for the middle ear. Chronic TM perforation is defined as perforation lasting 3 months [1]. Chronic perforation is often attributed to chronic inflammation of the purulent otitis media [2]. Since chronic otitis media can lead to serious or potentially fatal complications such as mastoiditis, facial nerve paresis, labyrinthitis, petrositis [3], meningitis, thrombophlebitis, and brain abscess [4]. Due to the reasons mentioned above, chronic otitis media can have a significant impact on a patient's quality of life [5]. This condition is estimated to impact between 65 and 330 million people worldwide, and causes major hearing impairment in over half of those affected with 21,000 fatalities annually [6]. Tympanoplasty is the most common surgical method in otorhinolaryngology surgery [7,8]. The tympanoplasty utilizes appropriate repair materials as a scaffold to assist the TM in self-healing, thereby restoring the normal structure of the perforated eardrum. The temporal muscle fascia

* Corresponding author.
** Corresponding author.
E-mail address: zxq@nimte.ac.cn (X. Zhang).

https://doi.org/10.1016/j.heliyon.2024.e31789
Received 12 February 2024; Received in revised form 21 May 2024; Accepted 22 May 2024
Available online 27 May 2024

and perichondrium are commonly used as repair materials because they can be easily collected from humans and have no risk of rejection. Tympanoplasty cured 94 % of instances of chronic otitis media, according to Caye-Thomasen et al.; Onal et al. observed that temporal fascia healed 65.9 % and chondrotympanoplasty treated 92.3 % of bilateral cases [9,10]. Nonetheless, the patients are at danger of infection at the surgical site and need to endure general anesthesia [11]. Otologists have attempted to reduce trauma and improve the success rate of the TM repair. So biomolecules and biomaterials have also been used in the regeneration of chronic TM perforations. At present, scaffold materials used for TM tissue engineering mainly include acellular scaffolds and polymer scaffolds. A decellularized scaffold is a natural structure extracted from natural organisms that removes cellular components and is highly structured and biocompatible. However, due to its limited plasticity and high cost, its application scope is limited. Polymer scaffolds are a more conducive scaffold material for human TM restoration. Polymers are divided into natural polymers and synthetic polymers. Synthetic polymers include polylactic acid, polycaprolactone, polysebacic acid glycerin, and aliphatic polycarbonate. Because of their great stability, lack of immunogenicity, capacity to continuously transport drugs, and enhanced drug bioavailability, synthetic polymers have found extensive use in the biomedical field [12]. Among them, aliphatic polycarbonate has recently received increasing attention due to its non-toxic nature, prominent biocompatibility and biodegradability [13-16].

Poly(1,4-butylene carbonate) (PBC) is an important member among the aliphatic polycarbonate. The high molecular weight PBC can be prepared by melt polycondensation of 1,4-butanediol and carbon dioxide-based raw material dimethyl carbonate. The melting temperature (T_m) of PBC ranged from 50 to 60 °C. It has excellent biodegradable properties, light weight, a high refractive index, good mechanical properties, good thermoplasticity, and is pollution-free to the environment [17]. PBC is easily decomposed under the action of heat, catalysts, or microorganisms, and the decomposition process can be controlled under certain conditions. Human mesenchymal stem/stromal cells (hMSCs) have been found to exhibit good adhesion and proliferation on printed PBC scaffolds, indicating that PBC scaffolds have good biocompatibility [17]. Furthermore, PBC scaffolds implanted in vivo can be degraded, and the main degradation products are butylene glycol and carbon dioxide [17].

In clinical care, topical or systemic antibiotics are usually used to prevent or control inflammation and infection in patients with TM perforation. Antibiotics can be given systemically or topically, and topical use is believed to be more beneficial in obtaining higher local concentrations of these drugs. However, traditional TM scaffolds, including PBC films, lack antimicrobial capabilities and cannot effectively address mixed infections in cases of TM perforation. Quinolone otic solutions have been shown to be effective in treating chronic suppurative otitis media with an improvement rate ranging from 65 % to 95 % in previous trials [18-21]. The most commonly found pathogenic organisms in otorrhea were *Staphylococcus* and *Pseudomonas*. Although the minimal inhibitory concentration 90 for LEV against *Staphylococcus* and *Pseudomonas* was high, with values of 64 μg/mL and >64 μg/mL, respectively, the eradication rates were high, with values of 83.3 % for *Staphylococcus* and 88.9 % for *Pseudomonas aeruginosa*. Thus, these results showed the effectiveness of topical administration [22]. Therefore, we chose to add LEV to PBC, which had never been studied in earlier research.

In this work, PBC/LEV films were successfully prepared by a chloroform solvent. Fourier transform infrared spectroscopy (FTIR) and X-Ray Diffraction were used to confirm whether new components were produced in the composite film. Thermal analysis and mechanical studies were conducted to test whether the PBC film conformed to the needed thermal properties and mechanical strength of the TM repair material. The hemolysis and cytotoxicity of the PBC films were determined by vitro hemolysis experiences and cytotoxicity assays. In addition, we further tested the antimicrobial activity of the PBC/LEV film against *Staphylococcus aureus* and *Pseudomonas aeruginosa*.

2. Materials and methods

2.1. Materials

Aladdin (Shanghai, China) provided levofloxacin (CAS: 100986-85-4, ≥98 %) and chloroform (C434286, 99.8 atom% D). 4 % rat red blood cell suspension was purchased from Nanjing SenBeiJia and Dulbecco's Modified Eagle's Medium(DMEM)was purchased from Thermo Fisher Scientific. Muller Hinton Agar was obtained from Zhengzhou Autobio. These were utilized exactly as supplied and required no additional purification. PBC with a weight-average molecular weight of 38,700 g/mol was provided by Ningbo Institute of Materials Technology and Engineering, Chinese Academy of Sciences.

2.2. Preparation of LEV/PBC films

An appropriate amount of PBC raw materials and a certain amount of LEV were weighed, dissolved in chloroform, and stirred magnetically for 24 h. After mixing fully, the solution was poured into a tetrafluoroethylene mold with dimensions of 10 cm × 6 cm × 0.5 cm (length × width × depth). After the chloroform volatilized, the films were formed and dried, with LEV concentrations of 0.5 wt %, 1 wt%, 3 wt% and a thickness of approximately 200 μm. At the same time, an appropriate amount of PBC raw material was also dissolved in chloroform, and a film (LEV containing 0 wt%) of the same size was prepared under the same conditions. The entire sample preparation procedure was performed at 50 % relative humidity and 25 °C. The PBC films with LEV contents of 0 wt%, 0.5 wt%, 1 wt%, and 3 wt% were successfully prepared (Supplementary Fig. 1). Then thermogravimetric-infrared spectroscopy (TG-IR) analysis was conducted to detect whether any chloroform remains in them. The obtained TGA curves and corresponding FTIR spectra at 61.1 °C and 61.3 °C are shown in Supplementary Fig. 2 and Supplementary Fig. 3. It is obvious that there is no weight loss around 61.2 °C, and no substance was detected in FTIR spectra, indicating no solvent was remained in all samples.

2.3. TG-IR analysis

TG-IR analyzer (TGA 8000-Spectrum two-Clarus SQ8T, PerkinElmer) was used to detect the residual presence of chloroform solvent in the sample. Approximately 8–9 mg of the sample was weighed and placed in a ceramic crucible. Under a nitrogen gas atmosphere, the temperature was ramped from 30 °C to 800 °C at a rate of 20 °C/min. The real-time monitoring of the sample's mass change and the structure of decomposition products were performed.

2.4. Morphological characterization

The prepared films were cut into squares measuring 0.5 cm × 0.5 cm. To observe the surface morphology, the film samples were coated with a thin layer of gold and then examined using scanning electron microscopy (SEM). The SEM imaging was performed using a high-resolution field emission scanning electron microscope (S-4800, Hitachi, Japan) at a magnification of 1000 × .

2.5. Fourier transform infrared (FTIR) spectroscopy

An attenuated total reflectance Fourier transform infrared (ATR-FTIR) spectrophotometer (Agilent Cary 600, USA) was used to analyze the chemical composition of the films. Furthermore, all spectra were obtained directly in transmittance mode using an accumulation of 64 scans with a resolution of 2 cm^{-1} on a diamond ATR crystal cell in the spectral region of 4000∼400 cm^{-1}.

2.6. Water contact angle measurement

Using the sessile drop method at room temperature and a video-based optical contact angle meter (Dataphysics OCA-25, Stuttgart, Germany), the water contact angle value of the membrane surface was measured. The samples were divided into pieces and positioned using double-sided tape on a glass slide. Using a microgauge, the droplet was applied to the sample surface. To measure the angle, 2 μL of deionized water was automatically added dropwise onto the sample surface. An average of three values from various sample places was used to determine each of the stated contact angles.

2.7. Thermal analysis

The thermal characteristics of PBC and PBC/LEV films were investigated using a differential scanning calorimetry (DSC) instrument (METTLER 3+, USA). The samples were tested in a nitrogen environment at a rate of 10 °C/min according to traditional heating-cooling-heating procedure, covering a temperature range from −70 to 180 °C. The heat flow of the composites was measured as a function of temperature.

2.8. Mechanical properties test

Stress-strain curves were obtained by measuring the load applied to dumbbell-shaped samples (with neck-width of 2 mm) using a universal material testing machine (Zwicki 1 kN, Germany). After being mounted in tensile grips, the sample thickness was determined using a digital caliper with a precision of 0.01 mm. The sample's test rate was 20 mm/min. The test was performed at room temperature. Each group of samples was tested 5 times.

2.9. X-ray diffraction

Using a high-power rotating target polycrystalline X-ray diffractometer (Bruker D8 Discover, Germany), the X-ray diffraction (XRD) patterns were acquired. Samples were scanned using Cu-Kα radiation (λ = 1.541 Å) at a scanning rate of 5.5°/min from 5° to 60°.

2.10. Hemolysis assays

In this study, hemolysis assays were conducted to evaluate the in vitro hemocompatibility of each PBC scaffold. A 4 % suspension of rat red blood cells was prepared and added to 1.5 mL centrifuge tubes. Round antibacterial films with a diameter of 6 mm were cut and placed into the tubes. The tubes were then incubated in a thermostatic cell culture incubator at 37 °C for a total of 2 h. Following incubation, the samples were centrifuged at 2000 rpm for 15 min, and the color and transparency of the supernatants from each group were observed after removal. An appropriate volume of supernatant was transferred to a 96-well plate, and the optical density (OD) was measured at 545 nm using a multifunction microplate spectrophotometer (Thermo Fisher Scientific, USA). The hemolysis rate of each group was calculated based on these measurements. The extent of red blood cell destruction determined the hemocompatibility of the fimls material. The experimental groups were defined as follows: (1) positive control group: 1 % Triton X-100; (2) blank control group: consisting of red blood cells and normal saline only; (3) PBC group; (4) PBC/LEV 0.5 wt% group; (5) PBC/LEV 1 wt% group; and (6) PBC/LEV 3 wt% group.

2.11. Cytotoxicity assay

The cytotoxicity of the films was evaluated by assessing cell viability. Circular pieces with a diameter of 14 mm were cut from each

film and sterilized. Subsequently, the sterilized films were placed onto a sterile 24-well culture plate, and DMEM cell culture medium was added. The films were pre-cultured overnight in a cell culture incubator. The next day, fibroblasts (ZQ 0450, Zhongqiao Xinzhou Biotech, Shanghai, China) in good growth status were seeded onto each film in the culture plate. After the cells adhered to the films and grew, the cell viability was tested every 24 h for approximately three days. Cell viability was measured using the Cell Counting Kit-8 (CCK-8) method. Specifically, 10 μL of CCK-8 solution was added to each well, and the cells were incubated for 2 h at 37 °C (n = 3). The control group consisted of cells grown without any film. After incubation, an appropriate volume of supernatant was transferred to a 96-well plate, and the OD was measured at 450 nm using a multifunction microplate spectrophotometer.

2.12. Antibacterial assay

The inhibition loop method was used to determine the antibacterial activity of each group of samples. Using the agar disk diffusion method, the antibacterial activity of the films against *Pseudomonas aeruginosa* (ATCC 27853, BLUEFBIO, Shanghai, China) and *Staphylococcus aureus* (ATCC 29213, BLUEFBIO, Shanghai, China) was assessed, and the inhibition zone (mm) was calculated. A suitable amount of bacteria with good survival status was picked from the culture medium using a sterile inoculation loop and transferred into sterile 0.85 % saline solution. The bacterial solution was adjusted to a McFarland turbidity of 0.5, corresponding to a bacterial concentration of approximately 1.5 × 10^8 cfu/mL. A volume of 100 μL of the bacterial suspension was dropped onto a sterile M − H agar plate, spread evenly using a sterile cotton swab, and left to stand for 10 min in a biosafety cabinet. Next, circular PBC films with a diameter of 6 mm were cut and sterilized with ultraviolet light. Each sterilized membrane was then attached to the center of the agar plate coated with bacterial suspension. After incubation at 37 °C in a constant temperature incubator for 24 h, the size of the inhibition zone was observed, photographed, and measured. Each experiment was repeated three times.

2.13. Statistical analysis

The experimental data were processed using Origin software and Graph Pad Prism, and data were presented as the mean ± standard deviation, with sample n = 3 or n = 5. The significance level was set at $p \leq 0.05$ by the ANOVA statistical test. Error bars represented the standard deviation.

3. Results and discussion

3.1. Morphology of LEV/PBC

For the microstructure analysis, Fig. 1 shows the SEM images after films formation. Fig. 1A shows the SEM image of the PBC film without LEV at 1000 magnification. The surface is relatively smooth and free of obvious particulate matter. However, after the addition

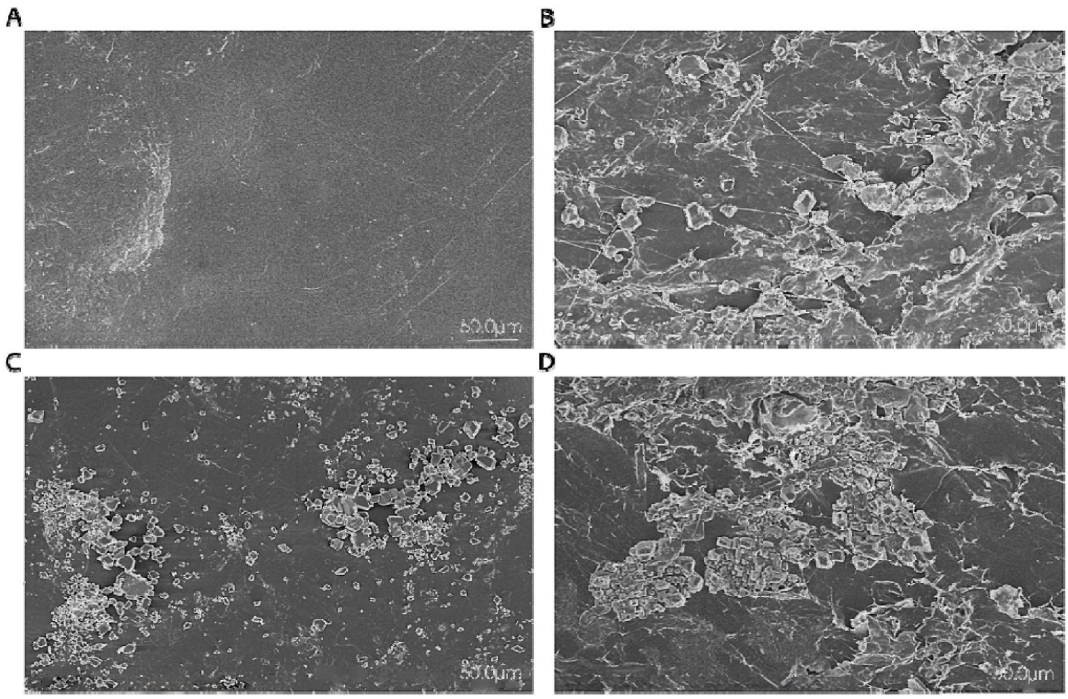

Fig. 1. SEM images of the film with different LEV contents at 1000 magnification. (A) 0 wt%; (B) 0.5 wt%; (C) 1 wt%; (D) 3 wt%.

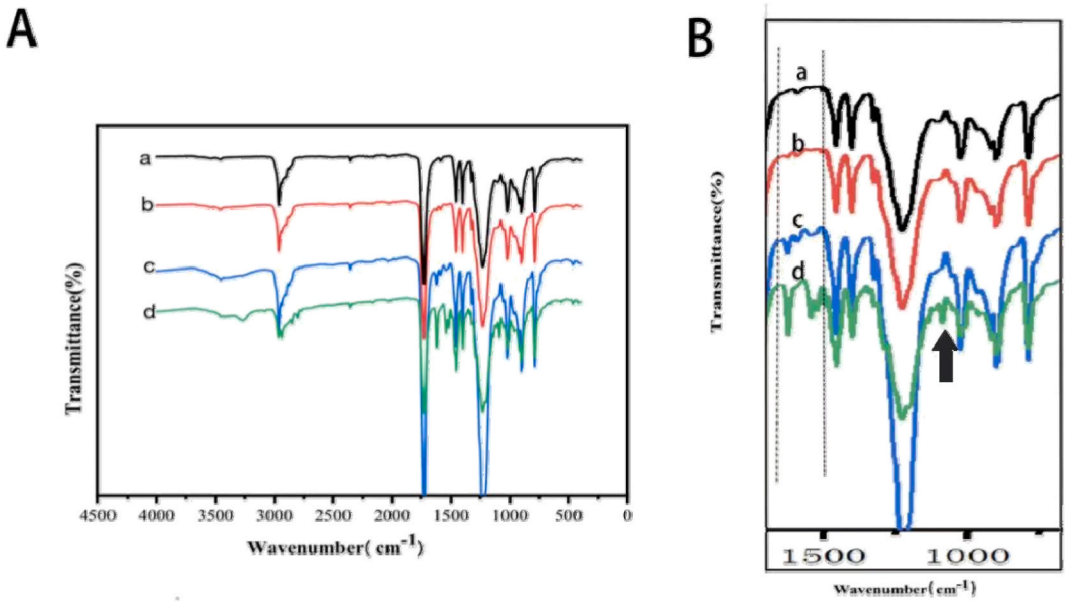

Fig. 2. (A) Infrared spectroscopy of the PBC films with different concentrations of LEV: a: PBC: (PBC films containing 0 wt% LEV). b: PBC composite films containing 0.5 wt% LEV; c: PBC composite films containing 1 wt% LEV; d: PBC composite films containing 3 wt% LEV. (B) Black arrow: characteristic peak caused by the F–C stretching vibration of LEV. Between two dotted lines: the characteristic peak of C═C in the benzene ring between 1500 and 1750 cm^{-1}.

of LEV to the PBC, electron microscopy revealed the presence of distinct particulate matter in the resulting film (Fig. 1B–D). At LEV contents below 1 %, LEV exhibits uniform distribution, whereas at a LEV content of 3 %, aggregation occurs due to LEV excess. It can be confirmed that LEV had been loaded on PBC surface successfully.

3.2. FTIR

From Fig. 2A, the stretching and bending vibrations at 790 and 900 cm^{-1} were attributed to the C–O bond and the C–H bond, respectively, and the stretching vibrations at 1226 cm^{-1} were attributed to the C–O or C–C bonds. Absorption at 1403 cm^{-1} is due to the stretching vibrations of the C–O or C–C bonds. The O–H stretching vibrations were observed between 2750 and 3000 cm^{-1}. The C═O stretching vibration occurs in the ranges of 2874–2898 cm^{-1} and 1710-1730 cm^{-1}. The N–H bending vibration occurs at 1584 cm^{-1}. The peak at approximately 3500 cm^{-1} was mainly caused by the superposition of O–H stretching vibrations. Comparing the infrared spectra of PBC/LEV composite films with different concentrations, the spectra of the four curves basically coincided, among which two curves (Fig. 2B, curves c and d) showed the characteristic peak of C═C from the benzene ring between 1500 and 1750 cm^{-1}, and the benzene ring is unique to LEV; this peak in curve d (Fig. 2B) was particularly evident. In addition, a weak peak was observed at 1022 cm^{-1} in the curve d (Fig. 2B) with a higher LEV concentration and was caused by the F–C stretching vibration of LEV (black arrow in Fig. 2B). This is similar to the detection results reported in previous studies by Han et al. using FTIR after the addition of LEV [23]. In summary, the chemical composition of the composite films and the composition of LEV did not change. This also showed the success of the preparation of composite films to a certain extent.

3.3. Water contact angle measurement

In this study, the hydrophilicity of PBC films with LEV contents of 0 wt%, 0.5 wt%, 1 wt%, and 3 wt% were compared by measuring the surface contact angle. The contact angle of the PBC film was found to be 101.69 ± 0.37° (Fig. 3A), indicating hydrophobicity and falling within the hydrophobic range. As depicted in Fig. 3B–D, the contact angles of PBC composite films with 0.5 wt%, 1 wt%, and 3 wt% LEV were measured to be 99.16 ± 1.23°, 96.12 ± 0.30°, and 95.59 ± 0.16°, respectively. This indicated that the hydrophilicity of the films increased with more and more added LEV. If the contact angle is greater than 90°, it indicates that the material is hydrophobic; If the contact angle is less than 90°, it indicates that the material is hydrophilic. So we can conclude that PBC films are hydrophobic materials. Previous studies have shown that cells tend to adhere, spread, and thrive better on moderately hydrophilic scaffolds rather than hydrophobic or highly hydrophilic scaffolds [24]. Hydrophobic materials have been utilized for supporting cell growth and tissue regeneration, providing good biocompatibility and mechanical properties while regulating cellular behavior for tissue repair and regeneration [25]. Hydrophobic scaffolds exhibit resistance to liquid attack, thereby maintaining scaffold shape and stability during the perforation healing process [26]. Additionally, the non-wetting surface of hydrophobic scaffolds reduces bacterial attachment and proliferation, consequently lowering the risk of infection [27].

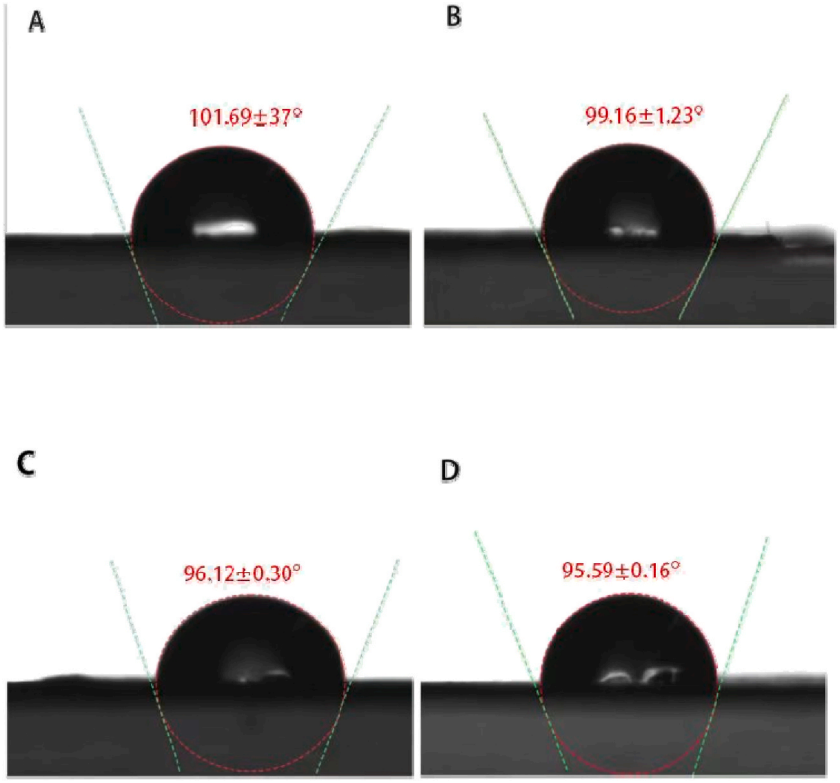

Fig. 3. Static water contact angle of the PBC films with LEV content in (A) 0 wt%; (B) 0.5 wt%; (C) 1 wt%; (D) 3 wt%.

3.4. Thermal analysis

The first and second DSC heating traces of PBC and PBC with LEV contents of 0.5 wt%, 1 wt%, and 3 wt% at 10 °C/min are illustrated in Fig. 4. The corresponding glass transition temperature (T_g), melting point (T_m), and melting enthalpy (ΔH_m) are shown in Table 1. From Fig. 4, it can be seen that the T_g and T_m of the samples before and after loading LEV slightly changed. The T_g ranged from −33.0 °C to −34.0 °C, while T_m distributed in 58.3–60.7 °C on their first heating curves (Fig. 4A) and in 58.1–58.8 °C on their second heating curves (Fig. 4B). All of these indicated that the drug did not form covalent bonds with PBC. At the same time, from the first heating curve, it can be seen that as the drug content increased, the triple endothermic peaks of PBC gradually disappear, and ΔH_m increases from 64.6 J/g for PBC to 71.4 J/g. It is speculated that the loaded drug may have played a role in inducing crystal nucleation, causing the crystallization of the samples to become perfect over time, and manifesting as a complete endothermic peak.

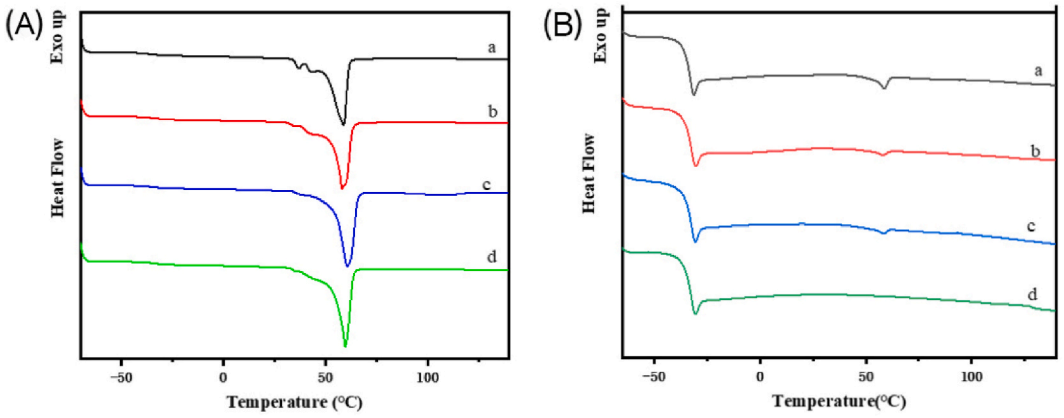

Fig. 4. DSC curves of the PBC films with different LEV contents (A) first heating scan, (B) second heating scan a: 0 wt%, b: 0.5 wt%, c: 1 wt%, d: 3 wt%.

Table 1
Thermal properties of PBC films with different LEV contents.

Sample	First heating scan				Second heating scan		
	T_{m1}	T_{m2}	T_{m3}	ΔH_m	T_g	T_m'	ΔH_m'
PBC	37.1	43.4	58.9	64.6	−34.0	58.8	0.4
0.5 wt%	34.9	42.5	58.3	67.5	−33.4	58.1	0.2
1 wt%	37.3	/	59.7	69.5	−33.0	58.4	0.3
3 wt%	/	/	60.7	71.4	−33.2	/	/

3.5. Mechanical properties

Fig. 5 shows the typical stress-strain curves of films with different LEV contents. When the content of LEV increased to 0.5 wt%, it exhibited enhanced tensile strength from 29.7 MPa of PBC to 32.6 MPa and reduced elongation at break from 286 % of PBC to 238 %. This could be caused by the introduction of a polar group, F, which potentially increased intermolecular forces and strength [23]. However, when the concentration of LEV increased to 1 wt% and 3 wt%, the opposite behavior occurred. This was because after the overloading of LEV on PBC, the PBC matrix structure was obviously destroyed, resulting in a decrease in the tensile strength. In addition, the tensile strength of the PBC film was 13.3–32.6 MPa, which was much higher than the 0.6–1.0 MPa of the human TM sample [28]. The specific mechanical properties of different PBC films are shown in Supplementary Table 1. The thickness of the human eardrum is about 0.1–0.2 mm, which makes the eardrum easy to vibrate and can transmit sound waves to the inner ear more efficiently [29]. The TM scaffold should also be relatively thin, so that it can better conform to the residual TM and reduce the loss of sound waves. During the TM repair operation, the TM scaffold will inevitably come into contact with the ossicle, and the thin TM scaffold is relatively light, which can reduce the large vibration of the ossicle. The thickness of the PBC scaffold prepared in this study is about 0.2 mm, which meets the requirements of TM scaffold. Due to the unique structure and function of the TM tissue, there are high demands on the material mechanics performance of TM scaffolds [30]. Good mechanical properties are essential to ensure that the scaffold can stably support and maintain the shape and structure of the TM. Tensile strength reflects the material's ability to resist fracture during stretching, with materials having high tensile strength being able to withstand pressure and vibrational elasticity at the site of TM perforation, thus reducing the risk of rupture. Additionally, ductility is one of the important indicators for evaluating the flexibility of materials. Better ductility provides the basis for materials to adapt to deformation at the perforation site [31]. Ideal materials for TM repair should be lightweight, thin [32], and have a certain level of impact resistance. Therefore, from the perspective of thickness and the corresponding mechanical properties of this thickness, the PBC films are suitable candidate for TM repair.

3.6. X-ray diffraction

XRD was used to determine the crystallization state of the sample, and the resulting XRD patterns are shown in Fig. 6. The XRD diffraction peaks of PBC appear at 20.7°and 21.2° in Fig. 6A. PBC/LEV0.5 %, PBC/LEV1%, and PBC/LEV3% exhibited the same diffraction peaks as pure PBC, indicating that the crystallization state of PBC was not affected by the addition of LEV. Similarly, the LEV was XRD tested with a spectrum as shown in Fig. 6B. The diffraction peaks at 6.6°and 26.3°of LEV were found on the XRD spectra of PBC/LEV 3 % (curve labeled "d" in Fig. 6A), indicating that LEV was successfully loaded on the surface of the PBC. However, the diffraction peaks of LEV at 9.7–19.4°could not be seen, because they were masked by the diffraction peaks of PBC in this range. The diffraction peaks of LEV are almost invisible in PBC/LEV0.5 % and PBC/LEV1%, which is mainly due to the fact that the amount of LEV

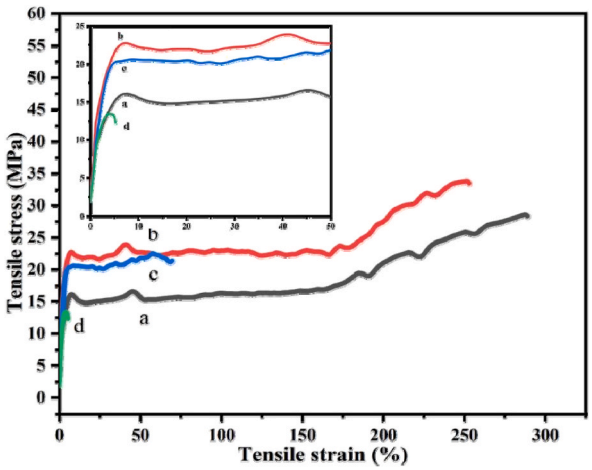

Fig. 5. Typical stress-strain curve of the PBC films with different LEV contents in the dry state. a: 0 wt%, b: 0.5 wt%, c: 1 wt%, d: 3 wt%.

added is too small to be detected. It can be determined that the LEV is successfully loaded on its surface without destroying the PBC state.

3.7. Hemolysis experiences

In this study, the blood compatibility from four sets of films was tested through in vitro hemolysis experiments. We cocultured four sets of films with 4 % rat red blood cell solution, with 1 % Triton X-100 as the positive control group and physiological saline as the negative control group. As shown in Fig. 7, after coculture with 4 % rat red blood cells for 3 h, we measured the absorbance of the supernatant in each group and further analyzed and compared the hemolysis rates of each group. The results showed that the hemolysis rates of the four groups of films were all below 5 %, demonstrating good blood compatibility. With the addition of LEV, the physical structure of the PBC scaffold changed, resulting in a decrease in the hemolysis rate. Due to the increase in the LEV content, the PBC films could not effectively fuse with LEV, and the LEV concentration in the blood could significantly increase, resulting in a slight increase in the hemolysis rate; however, this rate was also significantly lower than 5 %. Hemolysis tests are valuable in assessing haemocompatibility. When red blood cells encounter water or foreign substances, they can dissolve and release biomolecules such as hemoglobin due to osmotic pressure, and the damaged red blood cells attract platelets, accelerate blood clotting, and hinder tissue regeneration [25]. The ideal biomaterial should maintain the integrity of red blood cells and avoid triggering clotting while supporting tissue healing. In vitro hemolysis assay is a reliable and important index to evaluate the hemocompatibility of a material [33].

3.8. Cell viability and promotion

In this study, fibroblasts were seeded onto different groups of PBC films and co-cultured for 3 days. The viability of the cells was assessed using the CCK8 method to evaluate the flim's biocompatibility and cell proliferation. The experiment consisted of 5 groups, including a control group without PBC films, and experimental groups with PBC material concentrations of 0 wt%, 0.5 wt%, 1 wt%, and 3 wt% LEV. The results showed that on the first day of co-culture, the OD values of the cells in each group were similar, indicating good cell viability. As time progressed, the OD values continued to increase, suggesting that the films in each group had low toxicity and supported strong cell proliferation (Fig. 8). The above results indicated that all four films had good cell compatibility. Normal TM tissue is composed of the lateral keratosizing epithelium, the intermediate fibrous layer, and the medial mucosal epithelial layer, which as a whole contains many different types of cells, including fibroblasts, epithelial cells, endothelial cells, nerve cells, mucosal cells, mast cells, and various types of leukocytes and lymphocytes [34]. Fibroblasts are the main components of TM cells and the most important cells in the process of TM regeneration, and the TM scaffold should have good cytocompatibility, so we chose fibroblasts for the experiment [35].

3.9. Antibacterial properties

In this study, the sensitivity and bactericidal efficacy of each group of films to bacteria were analyzed and compared by measuring the size of their antibacterial zones against *Staphylococcus aureus* and *Pseudomonas aeruginosa*. As shown in Fig. 9, after culturing each group of films with equivalent bacteria for 24 h, no significant antibacterial circles were observed in the PBC films without LEV, indicating a lack of antibacterial ability. In contrast, the groups containing LEV all produced circular antibacterial circles centered around the films with clear edges. These results indicated that the films containing LEV had strong antibacterial activity. Usually, the size of the bacteriostatic zone is related to the release of LEV. A larger the bacteriostatic zone correlated to the release of more LEV. After comparison, the antibacterial zone areas of the 1 wt% LEV and 3 wt% LEV groups were significantly larger than that of the 0.5 wt % LEV group (Fig. 9). The specific measurement results are provided in Table 2. Each experiment was repeated 3 times, and from

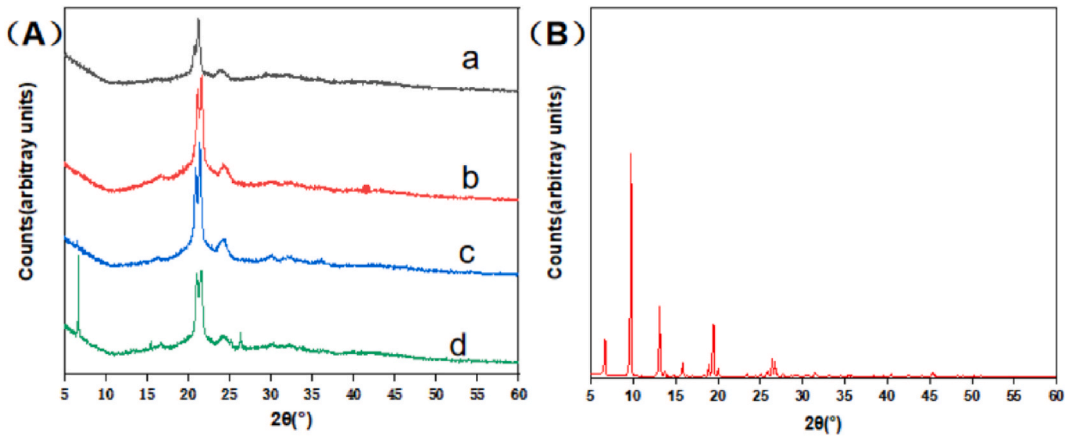

Fig. 6. A: The resulting XRD patterns of different PBC films. a: 0 wt%, b: 0.5 wt%, c: 1 wt%, d: 3 wt%.B:The spectrum of LEV was obtained via XRD.

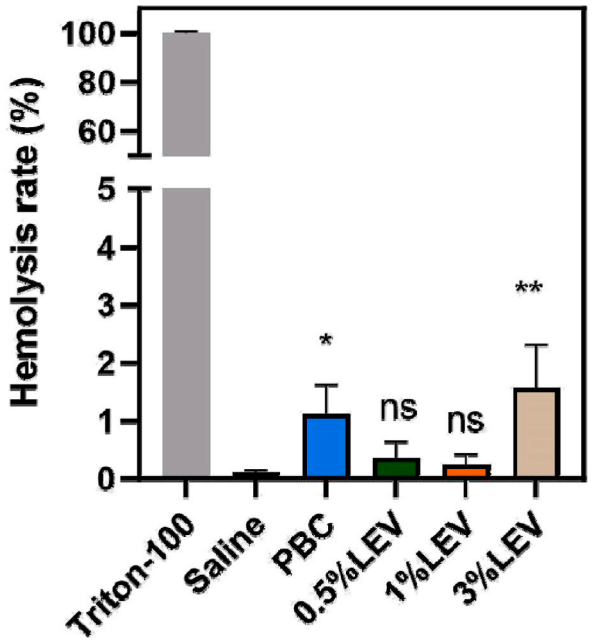

Fig. 7. Hemolysis rate of the PBC scaffold in each group. ns, *P < 0.05 and **P < 0.01 for saline vs. PBC, 0.5 wt%LEV, 1%wt%LEV and 3 wt%LEV.

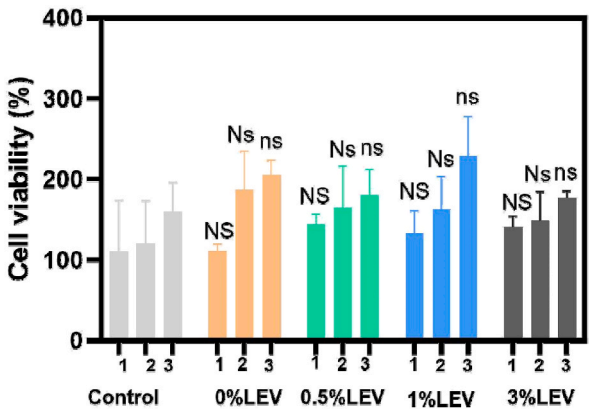

Fig. 8. Cell viability test of the fibroblasts cocultured with the PBC films for 3 days. NS just for control (1 day) vs. 0 wt%LEV, 0.5 wt%LEV, 1 wt% LEV, 3 wt%LEV; Ns just for control(2 day)vs. 0 wt%LEV, 0.5 wt%LEV, 1 wt%LEV, 3 wt%LEV; ns just for control (3 day) vs. 0 wt%LEV, 0.5 wt%LEV, 1 wt%LEV, 3 wt%LEV.

Table 2, we can find that the PBC film containing LEV has good antibacterial properties for both bacteria, and the higher the relative concentration, the better the antibacterial performance. The inhibition zones of PBC films with 0.5%wt, 1%wt, and 3%wt LEV against *Staphylococcus aureus* were 16.7 ± 1.2, 26.7 ± 2.9 and 30.7 ± *0.*6 mm, respectively (Fig. 9A). The inhibition zones of PBC films with 0.5%wt, 1%wt, and 3%wt LEV against *Pseudomonas aeruginosa* were 27.3 ± 1.1, 30.7 ± 2.5 and 34.0 ± 1.0 mm (Fig. 9B), respectively. *Staphylococcus aureus* and *Pseudomonas aeruginosa* are two of the most common pathogens in patients with clinical chronic OM [36]. Both types of bacteria can cause TM perforation through a variety of pathways, and after TM perforation occurs, both bacteria colonize the surface of the TM and release toxins and cytokines, which stimulate an inflammatory response in the TM tissue, resulting in a prolonged TM perforation that is difficult to heal. Among them, *Staphylococcus aureus* can release hemolytic toxins, induce potassium release from epithelial keratinocytes cause vasoconstriction [37], lead to capillary blood flow blockage and local ischemia necrosis in the TM, and if the perforation site is insufficient blood supply for a long time, growth will be arrested, which is not conducive to the regeneration of TM tissue. In addition, the virulence factors secreted by *Pseudomonas aeruginosa* can evade the phagocytosis of macrophages, induce leukocyte infiltration, cause autophagy in the TM tissue, exacerbate the inflammatory response of the tissue, and make it difficult for TM perforation to heal. Clinically, middle ear infections are usually treated with Lev ear drops to control middle ear infections [38]. Lev is an inexpensive and highly effective quinolone antibiotic with a broad spectrum of antimicrobial activity against a variety of common ear-causing bacteria, especially *Staphylococcus aureus* and *Pseudomonas aeruginosa* [23]. Through this experiment,

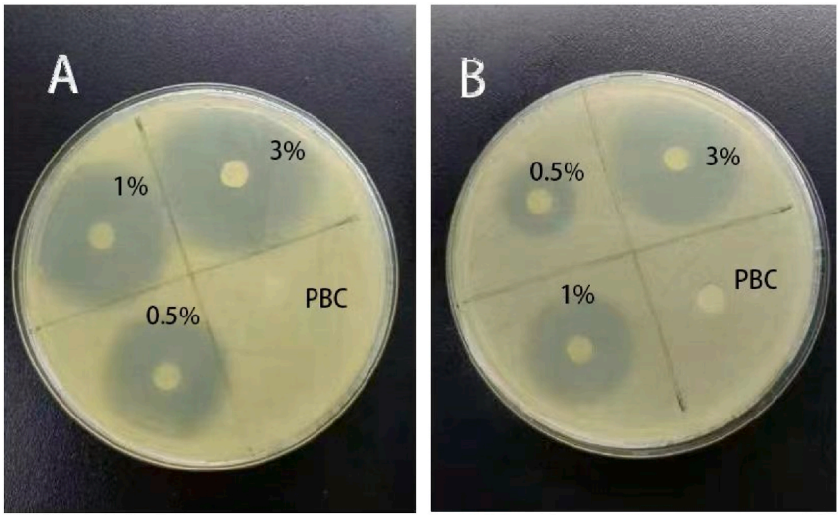

Fig. 9. Antibacterial circle diagram of the PBC films in (A) *Staphylococcus aureus* and (B) *Pseudomonas aeruginosa*.

Table 2
Inhibition zone diameters of the LEV/PBC films against.*Staphylococcus aureus* and *Pseudomonas aeruginosa*.

Bacteria	Inhibition zone (mm)			
	0%wtLEV	0.5%wtLEV	1%wtLEV	3%wtLEV
Staphylococcus aureus	ND	16.7 ± 1.2	26.7 ± 2.9	30.7 ± 0.6
Pseudomonas aeruginosa	ND	27.3 ± 1.1	30.7 ± 2.5	34.0 ± 1.0

ND = Not detected.

we can further demonstrate the success of antimicrobial PBC film preparation.

4. Conclusions

In this study, we prepared LEV loaded PBC composite films using a chloroform solution. SEM, FTIR, and XRD showed no significant chemical reaction between LEV and PBC. Contact angle experiments showed that the addition of LEV increased the hydrophilicity of the films, which is more favorable for cell adhesion, diffusion and growth. Through in vitro hemolysis and cytotoxicity experiments, we further demonstrated the non-toxicity of the PBC/LEV. Antibacterial experiments showed that PBC flims containing LEV exhibited certain antibacterial properties, with the 1 wt% and 3 wt% groups showing significantly superior antibacterial performance. Overall, our study preliminarily demonstrates the feasibility of using PBC/LEV films as a TM scaffold, providing important insights for future research on TM scaffolds.

Ethics approval and consent to participate

Not applicable.

Consent for publication

Not applicable.

Authors' contributions

YL, SZS contributed to the conception of the study. XQZ and LRW performed the data analyses and wrote the manuscript. YJY and JJZ helped to perform the experiment and contributed constructive discussions. LRW and TL collaborated to write and revise the article.

Availability of data and materials

The required experimental data can be obtained from the corresponding author.

Funding

Ningbo Top Medical and Health Research Program (No.2023030514); Ningbo Clinical Research Center for Otolaryngology Head and Neck Disease (No.2022L005); Ningbo "Technology Innovation 2025" Major Special Project (2020Z097); Medical and Health Research Project of Zhejiang Province (2024KY1481).

CRediT authorship contribution statement

Yuan Lv: Writing – review & editing, Conceptualization. **Linrong Wu:** Writing – original draft, Formal analysis, Data curation, Conceptualization. **Jiangyu Yan:** Writing – original draft, Formal analysis, Data curation. **Zhisen Shen:** Writing – review & editing, Conceptualization. **Junjun Zhang:** Formal analysis, Data curation. **Xiaoqin Zhang:** Writing – review & editing, Investigation, Formal analysis, Data curation. **Tian Li:** Writing – review & editing.

Declaration of competing interest

The authors declare that they have no known competing financial interests or personal relationships that could have appeared to influence the work reported in this paper.

Appendix A. Supplementary data

Supplementary data to this article can be found online at https://doi.org/10.1016/j.heliyon.2024.e31789.

References

[1] G.G. Browning, S. Gatehouse, The prevalence of middle ear disease in the adult British population, Clin. Otolaryngol. Allied Sci. 17 (1992) 317–321, https://doi.org/10.1111/j.1365-2273.1992.tb01004.x.
[2] D.H. Darrow, N. Dash, C.S. Derkay, Otitis media: concepts and controversies, Curr. Opin. Otolaryngol. Head Neck Surg. 11 (2003) 416–423, https://doi.org/10.1097/00020840-200312000-00002.
[3] T.-H. Yang, S. Xirasagar, Y.-F. Cheng, C.-S. Wu, Y.-W. Kao, B.-C. Shia, H.-C. Lin, Malignant otitis externa is associated with diabetes: a population-based case-control study, Ann. Otol. Rhinol. Laryngol. 129 (2020) 585–590, https://doi.org/10.1177/0003489419901139.
[4] Y.S. Lin, L.-C. Lin, F.-P. Lee, K.J. Lee, The prevalence of chronic otitis media and its complication rates in teenagers and adult patients, Otolaryngol. Head Neck Surg. 140 (2009) 165–170, https://doi.org/10.1016/j.otohns.2008.10.020.
[5] D. Lucidi, C. Cantaffa, R. Nocini, A. Martone, M. Alicandri-Ciufelli, D. Marchioni, L. Presutti, G. Molinari, Quality of life after surgical treatment for chronic otitis media: a systematic review of the literature, J. Personalized Med. 12 (2022) 1959, https://doi.org/10.3390/jpm12121959.
[6] L. Monasta, L. Ronfani, F. Marchetti, M. Montico, L. Vecchi Brumatti, A. Bavcar, D. Grasso, C. Barbiero, G. Tamburlini, Burden of disease caused by otitis media: systematic review and global estimates, PLoS One 7 (2012) e36226, https://doi.org/10.1371/journal.pone.0036226.
[7] C.-P. Li, L.-P. He, A study on the correlation between vocational self-efficacy and ego-identity in midwifery students, Alternative Ther. Health Med. 28 (2022) 153–157.
[8] W.N.A. Wan Draman, M.K. Md Daud, H. Mohamad, S.A. Hassan, N. Abd Rahman, Evaluation of the current bacteriological profile and antibiotic sensitivity pattern in chronic suppurative otitis media, Laryngoscope Invest. Otolaryngol. 6 (2021) 1300–1306, https://doi.org/10.1002/lio2.682.
[9] P. Caye-Thomasen, T.R. Nielsen, M. Tos, Bilateral myringoplasty in chronic otitis media, Laryngoscope 117 (2007) 903–906, https://doi.org/10.1097/MLG.0b013e318038168a.
[10] K. Onal, S. Arslanoglu, M. Songu, U. Demiray, I.A. Demirpehlivan, Functional results of temporalis fascia versus cartilage tympanoplasty in patients with bilateral chronic otitis media, J. Laryngol. Otol. 126 (2012) 22–25, https://doi.org/10.1017/S0022215111002817.
[11] M. Aleemardani, Z. Bagher, M. Farhadi, H. Chahsetareh, R. Najafi, B. Eftekhari, A. Seifalian, Can tissue engineering bring hope to the development of human tympanic membrane? Tissue Eng., Part B 27 (2021) 572–589, https://doi.org/10.1089/ten.TEB.2020.0176.
[12] H. A, S. Sofini P S, D. Balasubramanian, A. Girigoswami, K. Girigoswami, Biomedical applications of natural and synthetic polymer based nanocomposites, J. Biomater. Sci. Polym. Ed (2023) 1–44, https://doi.org/10.1080/09205063.2023.2283910.
[13] T. Ahlfeld, V. Guduric, S. Duin, A.R. Akkineni, K. Schütz, D. Kilian, J. Emmermacher, N. Cubo-Mateo, S. Dani, M.V. Witzleben, J. Spangenberg, R. Abdelgaber, R. F. Richter, A. Lode, M. Gelinsky, Methylcellulose - a versatile printing material that enables biofabrication of tissue equivalents with high shape fidelity, Biomater. Sci. 8 (2020) 2102–2110, https://doi.org/10.1039/d0bm00027b.
[14] S. Bandari, D. Nyavanandi, N. Dumpa, M.A. Repka, Coupling hot melt extrusion and fused deposition modeling: critical properties for successful performance, Adv. Drug Deliv. Rev. 172 (2021) 52–63, https://doi.org/10.1016/j.addr.2021.02.006.
[15] S. Heid, A.R. Boccaccini, Advancing bioinks for 3D bioprinting using reactive fillers: a review, Acta Biomater. 113 (2020) 1–22, https://doi.org/10.1016/j.actbio.2020.06.040.
[16] Z. Wan, P. Zhang, Y. Liu, L. Lv, Y. Zhou, Four-dimensional bioprinting: current developments and applications in bone tissue engineering, Acta Biomater. 101 (2020) 26–42, https://doi.org/10.1016/j.actbio.2019.10.038.
[17] Y.B. Ji, J.Y. Park, Y. Kang, S. Lee, H.J. Ju, S. Choi, B.Y. Lee, M.S. Kim, Scaffold printing using biodegradable poly(1,4-butylene carbonate) ink: printability, in vivo physicochemical properties, and biocompatibility, Mater. Today Bio. 12 (2021) 100129, https://doi.org/10.1016/j.mtbio.2021.100129.
[18] I. Kaygusuz, T. Karlidağ, U. Gök, S. Yalçin, E. Keleş, E. Demirbağ, T.O. Kaygusuz, [Efficacy of topical ciprofloxacin and tobramycin in combination with dexamethasone in the treatment of chronic suppurative otitis media], Kulak Burun Bogaz Ihtis. Derg. 9 (2002) 106–111.
[19] C. Macfadyen, C. Gamble, P. Garner, I. Macharia, I. Mackenzie, P. Mugwe, H. Oburra, K. Otwombe, S. Taylor, P. Williamson, Topical quinolone vs. antiseptic for treating chronic suppurative otitis media: a randomized controlled trial, Trop. Med. Int. Health 10 (2005) 190–197, https://doi.org/10.1111/j.1365-3156.2004.01368.x.
[20] O. Nawasreh, A. Fraihat, Topical ciprofloxacin versus topical gentamicin for chronic otitis media, East. Mediterr. Health J. 7 (2001) 26–30.
[21] A. Ramos, F. Ayudarte, I. de Miguel, J.M. Cuyás, C. Cenjor, Use of topical ciprofloxacin in chronic suppurating otitis media, Acta Otorrinolaringol. Esp. 54 (2003) 485–490, https://doi.org/10.1016/s0001-6519(03)78439-8.

[22] K. Suzuki, Y. Kurono, K. Ikeda, M. Hotomi, H. Yano, A. Watanabe, T. Matsumoto, Y. Takahashi, H. Hanaki, The seventh nationwide surveillance of six otorhinolaryngological infectious diseases and the antimicrobial susceptibility patterns of the isolated pathogens in Japan, J. Infect. Chemother. 26 (2020) 890–899, https://doi.org/10.1016/j.jiac.2020.05.020.
[23] S. Han, Z. Zhang, J. Chen, J. Li, M. Zhou, Z. He, Z. He, L. Li, Preparation of antibacterial gelatin/genipin nanofibrous membrane for tympanic membrane repair, Molecules 27 (2022) 2906, https://doi.org/10.3390/molecules27092906.
[24] E.D. Kozin, N.L. Black, J.T. Cheng, M.J. Cotler, M.J. McKenna, D.J. Lee, J.A. Lewis, J.J. Rosowski, A.K. Remenschneider, Design, fabrication, and in vitro testing of novel three-dimensionally printed tympanic membrane grafts, Hear. Res. 340 (2016) 191–203, https://doi.org/10.1016/j.heares.2016.03.005.
[25] X. Peng, Y. Li, T. Li, Y. Li, Y. Deng, X. Xie, Y. Wang, G. Li, L. Bian, Coacervate-derived hydrogel with effective water repulsion and robust underwater bioadhesion promotes wound healing, Adv. Sci. (Weinh) 9 (2022) e2203890, https://doi.org/10.1002/advs.202203890.
[26] E. Krok, H.G. Franquelim, M. Chattopadhyay, H. Orlikowska-Rzeznik, P. Schwille, L. Piatkowski, Nanoscale structural response of biomimetic cell membranes to controlled dehydration, Nanoscale 16 (2023) 72–84, https://doi.org/10.1039/d3nr03078d.
[27] K.W.J. Verhorstert, Z. Guler, L. de Boer, M. Riool, J.-P.W.R. Roovers, S.A.J. Zaat, In vitro bacterial adhesion and biofilm formation on fully absorbable poly-4-hydroxybutyrate and nonabsorbable polypropylene pelvic floor implants, ACS Appl. Mater. Interfaces 12 (2020) 53646–53653, https://doi.org/10.1021/acsami.0c14668.
[28] G. Ajmal, G.V. Bonde, P. Mittal, G. Khan, V.K. Pandey, B.V. Bakade, B. Mishra, Biomimetic PCL-gelatin based nanofibers loaded with ciprofloxacin hydrochloride and quercetin: a potential antibacterial and anti-oxidant dressing material for accelerated healing of a full thickness wound, Int. J. Pharm. 567 (2019) 118480, https://doi.org/10.1016/j.ijpharm.2019.118480.
[29] S.-Y. Zhou, L. Li, E. Xie, M.-X. Li, J.-H. Cao, X.-B. Yang, D.-Y. Wu, Small-diameter PCL/PU vascular graft modified with heparin-aspirin compound for preventing the occurrence of acute thrombosis, Int. J. Biol. Macromol. 249 (2023) 126058, https://doi.org/10.1016/j.ijbiomac.2023.126058.
[30] M.A. Villar-Fernandez, J.A. Lopez-Escamez, Outlook for tissue engineering of the tympanic membrane, Audiol. Res. 5 (2015) 117, https://doi.org/10.4081/audiores.2015.117.
[31] K. Lu, Nanomaterials. Making strong nanomaterials ductile with gradients, Science 345 (2014) 1455–1456, https://doi.org/10.1126/science.1255940.
[32] C.-F. Lee, J.-H. Chen, Y.-F. Chou, L.-P. Hsu, P.-R. Chen, T.-C. Liu, Optimal graft thickness for different sizes of tympanic membrane perforation in cartilage myringoplasty: a finite element analysis, Laryngoscope 117 (2007) 725–730, https://doi.org/10.1097/mlg.0b013e318031f0e7.
[33] X. Zhang, J. Feng, W. Feng, B. Xu, K. Zhang, G. Ma, Y. Li, M. Yang, F.-J. Xu, Glycosaminoglycan-based hydrogel delivery system regulates the wound microenvironment to rescue chronic wound healing, ACS Appl. Mater. Interfaces 14 (2022) 31737–31750, https://doi.org/10.1021/acsami.2c08593.
[34] K. Stenfeldt, C. Johansson, S. Hellström, The collagen structure of the tympanic membrane: collagen types I, II, and III in the healthy tympanic membrane, during healing of a perforation, and during infection, Arch. Otolaryngol. Head Neck Surg. 132 (2006) 293–298, https://doi.org/10.1001/archotol.132.3.293.
[35] L.J. Liew, L.Q. Chen, A.Y. Wang, M. von Unge, M.D. Atlas, R.J. Dilley, Tympanic membrane derived stem cell-like cultures for tissue regeneration, Stem Cell. Dev. 27 (2018) 649–657, https://doi.org/10.1089/scd.2018.0021.
[36] A. Coleman, A. Wood, S. Bialasiewicz, R.S. Ware, R.L. Marsh, A. Cervin, The unsolved problem of otitis media in indigenous populations: a systematic review of upper respiratory and middle ear microbiology in indigenous children with otitis media, Microbiome 6 (2018) 199, https://doi.org/10.1186/s40168-018-0577-2.
[37] K.R. Kirker, P.R. Secor, G.A. James, P. Fleckman, J.E. Olerud, P.S. Stewart, Loss of viability and induction of apoptosis in human keratinocytes exposed to Staphylococcus aureus biofilms in vitro, Wound Repair Regen. 17 (2009) 690–699, https://doi.org/10.1111/j.1524-475X.2009.00523.x.
[38] K. Gjødsbøl, J.J. Christensen, T. Karlsmark, B. Jørgensen, B.M. Klein, K.A. Krogfelt, Multiple bacterial species reside in chronic wounds: a longitudinal study, Int. Wound J. 3 (2006) 225–231, https://doi.org/10.1111/j.1742-481X.2006.00159.x.